NEUROSCIENCE

Cortical-subcortical structural connections support transcranial magnetic stimulation engagement of the amygdala

Valerie J. Sydnor[1,2], Matthew Cieslak[1,2], Romain Duprat[3], Joseph Deluisi[3], Matthew W. Flounders[3], Hannah Long[3], Morgan Scully[3], Nicholas L. Balderston[3], Yvette I. Sheline[3], Dani S. Bassett[2,4,5,6,7,8], Theodore D. Satterthwaite[1,2,9], Desmond J. Oathes[3,10]*

Copyright © 2022 The Authors, some rights reserved; exclusive licensee American Association for the Advancement of Science. No claim to original U.S. Government Works. Distributed under a Creative Commons Attribution NonCommercial License 4.0 (CC BY-NC).

The amygdala processes valenced stimuli, influences emotion, and exhibits aberrant activity across anxiety disorders, depression, and PTSD. Interventions modulating amygdala activity hold promise as transdiagnostic psychiatric treatments. In 45 healthy participants, we investigated whether transcranial magnetic stimulation (TMS) elicits indirect changes in amygdala activity when applied to ventrolateral prefrontal cortex (vlPFC), a region important for emotion regulation. Harnessing in-scanner interleaved TMS/functional MRI (fMRI), we reveal that vlPFC neurostimulation evoked acute and focal modulations of amygdala fMRI BOLD signal. Larger TMS-evoked changes in the amygdala were associated with higher fiber density in a vlPFC–amygdala white matter pathway when stimulating vlPFC but not an anatomical control, suggesting this pathway facilitated stimulation-induced communication between cortex and subcortex. This work provides evidence of amygdala engagement by TMS, highlighting stimulation of vlPFC–amygdala circuits as a candidate treatment for transdiagnostic psychopathology. More broadly, it indicates that targeting cortical-subcortical structural connections may enhance the impact of TMS on subcortical neural activity and, by extension, subcortex-subserved behaviors.

INTRODUCTION

The amygdala is a critical neural structure for determining an individual's physiological, emotional, and behavioral responses to affective stimuli. This medial temporal subcortical brain region assigns valence to rewards and threats, facilitates appetitive and aversive conditioning, and influences positive and negative internal emotional states as well as associated behaviors (*1*–*4*). Conscious recognition and regulation of amygdala-linked emotional states recruits the prefrontal cortex (PFC), including ventrolateral PFC (vlPFC) areas subserving emotional control and reappraisal (*5*–*11*). Aberrant activity within the amygdala and the vlPFC contributes to symptoms of psychopathology observed across many psychiatric diagnoses (*11*–*14*). Indeed, a meta-analysis of task functional magnetic resonance imaging (fMRI) data collected from more than 11,000 individuals revealed that, during emotional processing, patients with mood, anxiety, and stress disorders consistently exhibit amygdala hyperactivity and vlPFC hypoactivity—classifying these as two of the most notable and reliable neural phenotypes associated with emotion dysregulation (*11*). Treatments capable of modulating amygdala activity, especially those that simultaneously engage the vlPFC, therefore hold promise for mitigating transdiagnostic symptoms of emotional-related psychopathology.

Transcranial magnetic stimulation (TMS) is a noninvasive neuromodulation tool that produces changes in neural firing through electromagnetic induction and that may be capable of eliciting indirect changes in amygdala activity through direct stimulation of functionally or structurally connected cortical locations. Clinically, repetitive TMS administered to the PFC is U.S. Food and Drug Administration–cleared as a treatment for medication-resistant major depression and obsessive compulsive disorder, and has been studied in clinical trials for posttraumatic stress disorder and anxiety disorders (*15*, *16*)—all disorders characterized by amygdala hyperactivity (*11*, *13*, *14*, *17*). Still, despite the demonstrated efficacy for many patients, clinical responses to TMS are variable and not all individuals experience symptom remission. Recent work suggests that the efficacy of prefrontal TMS for mood, anxiety, and stress disorders may depend, in part, upon the strength of PFC-amygdala functional connections (*18*–*20*), further suggesting that efficacy may vary according to TMS's ability to alter amygdala functioning. However, to date, there is limited direct evidence that prefrontal TMS can specifically modulate amygdala activity (*18*, *21*, *22*). Furthermore, the extent to which TMS applied to the vlPFC is capable of evoking immediate, reliable changes in amygdala activity remains sparsely investigated, despite the fact that this psychopathology-linked cortical territory is hypothesized to exert top-down control over amygdala neuronal firing (*6*, *10*).

TMS alters neural activity by depolarizing somas and large-diameter axons, generating action potentials (*23*). Although TMS can only directly depolarize neurons at the cortical surface beneath the device's magnetic coil (*24*), empirical evidence suggests that TMS can additionally elicit indirect activity changes in "downstream" regions.

[1]Penn Lifespan Informatics and Neuroimaging Center (PennLINC), Perelman School of Medicine, University of Pennsylvania, Philadelphia, PA 19104, USA. [2]Department of Psychiatry, Perelman School of Medicine, University of Pennsylvania, Philadelphia, PA 19104, USA. [3]Center for Neuromodulation in Depression and Stress (CNDS), Department of Psychiatry, Perelman School of Medicine, University of Pennsylvania, Philadelphia, PA 19104, USA. [4]Department of Bioengineering, School of Engineering and Applied Science, University of Pennsylvania, Philadelphia, PA 19104, USA. [5]Department of Electrical and Systems Engineering, School of Engineering and Applied Science, University of Pennsylvania, Philadelphia, PA 19104, USA. [6]Department of Physics and Astronomy, College of Arts and Sciences, University of Pennsylvania, Philadelphia, PA 19104, USA. [7]Department of Neurology, Perelman School of Medicine, University of Pennsylvania, Philadelphia, PA 19104, USA. [8]Santa Fe Institute, Santa Fe, NM 87501, USA. [9]Center for Biomedical Image Computing and Analytics (CBICA), University of Pennsylvania, Philadelphia, PA 19104, USA. [10]Penn Brain Science, Translation, Innovation, and Modulation Center (brainSTIM), Perelman School of Medicine, University of Pennsylvania, Philadelphia, PA 19104, USA.
*Corresponding author. Email: oathes@pennmedicine.upenn.edu

Perhaps the strongest evidence of this phenomenon comes from motor-evoked potentials: hand muscle electrical potentials recorded in response to TMS of the contralateral motor cortex. These potentials establish that TMS-induced action potentials can propagate along multisynaptic axonal pathways to elicit activity distant from the cortical site of stimulation (*23*). Additional empirical evidence is provided by studies combining TMS with invasive electrode recordings (*25*) or noninvasive fMRI recordings (*26*) that have revealed how TMS-induced activity can propagate throughout the brain in a pattern predicted by the stimulated cortex's structural connectome (*27*).

Combining TMS with fMRI represents a powerful experimental manipulation method, as single pulses of TMS (spTMS) can be delivered inside the MRI scanner interleaved with fMRI functional readouts (spTMS/fMRI). Accordingly, spTMS/fMRI allows one to alter neural activity underneath the TMS coil with stimulation probes while quantitatively measuring effects in the rest of the brain, including in subcortex, constituting a causal "probe-and-measure" approach (*26*, *28*). The success of this approach is underpinned by compatibility between TMS-elicited physiological responses and fMRI acquisition properties. Specifically, TMS-elicited changes in neural activity are reliably captured by hemodynamic changes (*24*), which drive the fMRI blood oxygen level–dependent (BOLD) signal. The acute fMRI BOLD response to TMS takes several seconds to peak; thus, a time delay can be incorporated before the fMRI readout to prevent compromising functional recordings. Moreover, single pulses of TMS briefly evoke neural activity without exerting cumulative effects on firing (*28*), enabling the averaging of single trial fMRI responses to TMS.

In a recent pilot study, our group used spTMS/fMRI while stimulating a spatially diverse range of lateral PFC sites, and demonstrated feasibility for TMS to evoke downstream changes in the fMRI BOLD signal in the subgenual anterior cingulate cortex and the amygdala (*22*). Critically, in this pilot, we observed that stimulation of sites located within or near the vlPFC produced the largest decreases in amygdala BOLD signal. Rhesus macaque tract-tracing work has shown that while the medial PFC is extensively connected to the amygdala (*29*), most lateral PFC areas are only lightly connected, with the exception of the vlPFC (*7*). The vlPFC sends dense, monosynaptic inputs to the amygdala, and thus is the only PFC region with a substantial (as opposed to sparse) amygdala projection that is directly accessible to TMS (*7*, *10*). These data support the hypothesis that vlPFC TMS may be particularly capable of modulating amygdala activity due to stimulation-induced action potential propagation along vlPFC-to-amygdala white matter connections. However, vlPFC–amygdala structural connections have been scarcely studied in humans (*30*). It therefore remains unknown whether they could comprise one key pathway for cortical-amygdala signal propagation during neuromodulation.

The current study endeavored to causally interrogate whether TMS can exert neuromodulatory effects on the amygdala through the engagement of cortical-subcortical structural pathways. To accomplish this, we first used a stimulation-based probe-and-measure approach to validate our initial finding that stimulation applied near the vlPFC ("probe") elicits an acute functional response in the amygdala ("measure"). We next sought to elucidate the structural scaffolding that could allow cortical stimulation to generate a targeted downstream amygdala response. We expected to identify a vlPFC-to-amygdala white matter pathway that is homologous between human and nonhuman primates; moreover, we hypothesized that pathway properties influencing signal conduction would affect the degree to which TMS affected amygdala activity. The results of our study can be harnessed to develop TMS protocols for modulating cortical-amygdalar circuits involved in transdiagnostic emotion-related psychopathology. Extension of these results to patient populations may facilitate the translation of amygdala-targeting TMS to therapeutic clinical trials.

RESULTS

We leveraged a unique, multimodal dataset to causally probe amygdala fMRI responses to cortical stimulation and to retrospectively investigate whether the magnitude of the response was associated with structural properties of cortical-amygdala white matter connections (Fig. 1). This dataset consisted of resting-state fMRI, structural and diffusion MRI, and in-scanner interleaved spTMS/fMRI data collected from 45 healthy individuals ages 18 to 55 years (mean age 28 ± 8.6 years; 27 female). This sample of participants was nonoverlapping with our pilot TMS/fMRI sample (*22*). To study how noninvasive cortical stimulation affects the amygdala, we applied pulses of TMS in the scanner to individual-specific stimulation sites informed by functional connectivity, and examined fMRI readouts

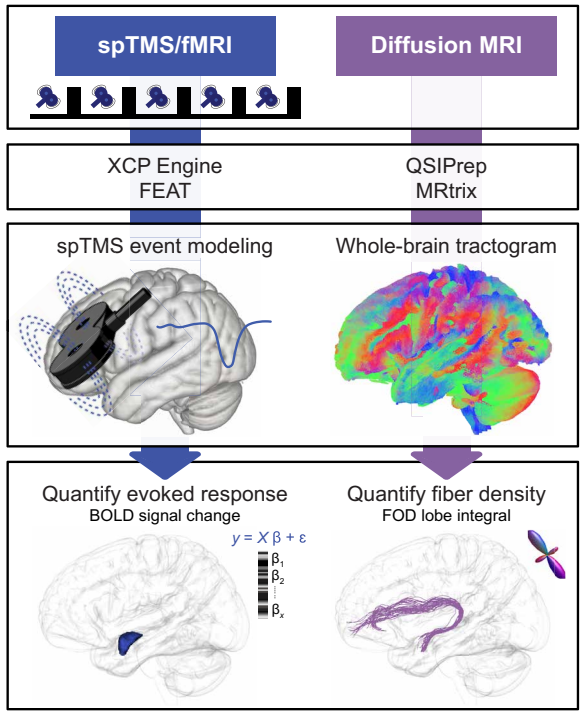

Fig. 1. Multimodal analysis workflows. spTMS/fMRI: Single pulses of TMS was administered in between fMRI volume acquisitions. TMS pulses were delivered to fMRI-guided, personalized left prefrontal sites of stimulation. Functional time series were analyzed with the FMRI Expert Analysis Tool (FEAT) via eXtensible Connectivity Pipeline (XCP) Engine's task module; each TMS pulse was modeled as an instantaneous event. TMS evoked responses were quantified in the left amygdala for each participant by averaging event-related BOLD signal changes induced by stimulation. Diffusion MRI: Diffusion data were preprocessed with QSIPrep. Preprocessed images were reconstructed with MRtrix's single-shell three-tissue constrained spherical deconvolution pipeline to generate FOD images. A whole-brain tractogram was then generated with FOD tractography. A structural pathway connecting the left amygdala to the prefrontal area of TMS stimulation was isolated, and pathway fiber density was quantified.

in the subcortex. To explore links between amygdala spTMS/fMRI functional responses and cortical-subcortical structural connectivity, we reconstructed white matter connections between the area of stimulation and the amygdala using fiber orientation distribution (FOD) tractography.

vlPFC TMS modulates fMRI BOLD activity in the amygdala

We used in-scanner interleaved spTMS/fMRI to replicate our prior preliminary study (*22*) in a larger, independent sample and confirm that cortical stimulation exerts neuromodulatory effects on the amygdala, our downstream target of interest. For each participant, a personalized left prefrontal TMS site of stimulation was chosen, which exhibited strong functional connectivity to the left amygdala (based on resting fMRI; see Materials and Methods) and which was located within, or in closest proximity to, the vlPFC. A functional connectivity–guided approach was used in light of prior evidence that cortical TMS will elicit larger biobehavioral changes associated with a downstream region, if that region is strongly functionally connected to the cortical stimulation site (*22*, *31*–*35*). We focused on the left PFC as there is abundant evidence demonstrating the safety and efficacy of TMS to this area for symptom reduction in psychiatric disorders (*15*, *16*). High functional connectivity sites nearest to the left vlPFC, in particular, were given priority based on our pilot study (*22*), the accessibility of this cortical area to TMS, and primate tract-tracing work (*7*). Accordingly, most individual-specific stimulation sites were located directly within the vlPFC, although a select number of functional connectivity–guided TMS sites fell outside of the anatomical vlPFC within more dorsal prefrontal areas (Fig. 2A).

To empirically assess the impact of spTMS on ipsilateral amygdala activity, we measured the percent change in BOLD signal elicited by stimulation events, relative to an implicit baseline of no stimulation. We refer to this TMS-evoked change in the fMRI BOLD signal as the TMS "evoked response." The TMS evoked response is negative when pulses of neurostimulation produce time-locked reductions in the fMRI BOLD signal. The TMS evoked response is positive when stimulation pulses elicit increases in the fMRI BOLD signal. Both positive and negative amygdala evoked responses provide evidence of a transient change in subcortical activity in response to cortical stimulation, and therefore evidence for a cortical-subcortical pathway supporting TMS signal propagation. The direction of the signed evoked response and the overall amplitude of the unsigned evoked response provide complementary information on the nature and the strength of TMS effects in the subcortex. Here, we investigate both the signed TMS evoked response, defined as the raw positive or negative percent change in BOLD signal, and the magnitude of the evoked response, defined as the size of the absolute value of the response.

Across the 45 study participants, the average magnitude of the left amygdala evoked response was 0.21% ± 0.14. A BOLD signal change of 0.20% is comparable in magnitude to BOLD effects produced by tasks that functionally engage the amygdala (*36*–*38*), indicating that spTMS applied to cortically accessible sites elicited a functional response in the amygdala. Examining the direction of each participant's TMS evoked response revealed that TMS pulses decreased BOLD signal in the left amygdala in 30 of 45 individuals (Fig. 2B), a directional effect that is potentially indicative of amygdala deactivation. As a result, the population estimated signed TMS evoked response was negative and significantly different from 0 [average signed evoked response = −0.09% ± 0.24, t_{44} = −2.51, Cohen's d = 0.37, 95% confidence interval (CI) = [−0.16 to −0.02], P = 0.0160], consistent with the idea that stimulation pulses tended to inhibit amygdala activity. We conducted a preliminary analysis of evoked response directionality across three subdivisions of the amygdala based on boundaries defined by a probabilistic histological atlas (fig. S1). The signed TMS evoked response was significant and negative for the left basolateral amygdala (average signed evoked response = −0.12% ± 0.22, t_{44} = −3.51, Cohen's d = 0.52, 95% CI = [−0.18 to −0.05], P_{FDR} = 0.0031), but not significant for left superficial or centromedial amygdala subdivisions (average signed evoked response = −0.06 and 0.05%, respectively, P_{FDR} = 0.1701 and 0.2531). Hence, response directionality was most homogeneous in the basolateral amygdala, with 75% of participants showing a pattern of TMS-induced decrease in BOLD signal in this area, which likely contributed to the overall amygdala directional effect.

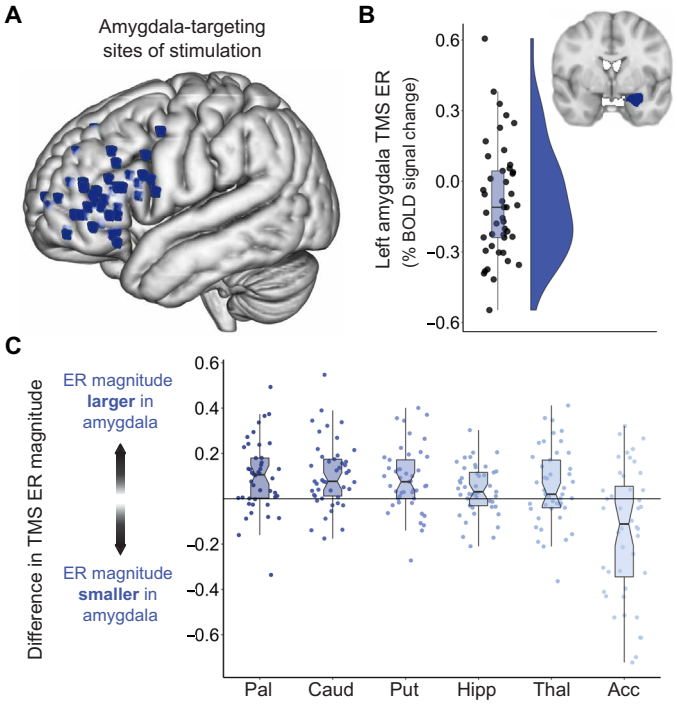

Fig. 2. Amygdala BOLD signal change following TMS administered to vlPFC connectivity peaks. (**A**) Each participant's amygdala-targeting TMS stimulation site visualized in standard (MNI) space. Individual-specific stimulation sites were localized to a left prefrontal area that was strongly functionally connected to the left amygdala and that was located directly within the vlPFC, or in closest proximity to the vlPFC of all connectivity peaks. (**B**) TMS elicited a sizable fMRI response in the ipsilateral amygdala. The signed TMS evoked response (TMS ER) in the left amygdala is plotted for all participants, along with corresponding box and violin plots. TMS pulses delivered to connectivity-informed stimulation sites decreased BOLD signal in the amygdala for most participants, as indicated by negative TMS ERs. (**C**) To assess whether amygdala-targeted TMS elicited larger functional responses in the left amygdala than in non-targeted subcortical structures, the magnitude of the TMS ER was compared between the amygdala and the left pallidum (Pal), caudate (Caud), putamen (Put), hippocampus (Hipp), thalamus (Thal), and nucleus accumbens (Acc). For each participant, the absolute valued TMS ER in these six control structures was subtracted from the absolute valued TMS ER in the amygdala, and the difference in TMS ER magnitude was plotted. Data points falling above the $y = 0$ line indicate that a participant had a larger amplitude TMS ER in the amygdala than in the indicated subcortical region.

Next, to ascertain whether individual-tailored aspects of the stimulation protocol influenced left amygdala evoked response direction, we considered whether response direction was related to TMS stimulation site functional connectivity or anatomical position. Functional connectivity strength between the stimulation site and the left amygdala did not differ between participants that exhibited a negative versus a positive left amygdala TMS evoked response (t_{43} = 0.17, Cohen's d = 0.05, 95% CI = [−0.08 to 0.09], P = 0.8683). Negative and positive evoked response groups also did not differ in how anteriorly (t_{43} = −0.80, Cohen's d = 0.25, 95% CI = [−5.85 to 2.52], P = 0.4264) or ventrally (t_{43} = 0.66, 95%, Cohen's d = 0.21, 95% CI = [−2.83 to 5.56], P = 0.5146) TMS was applied, as determined by stimulation site Y and Z coordinates in standard space. These three factors were moreover not continuously related to the signed TMS evoked response (Spearman's correlations, all P > 0.05). Variability in downstream, intrinsic responses to TMS could thus not be readily predicted from cortical stimulation site features, although notably all sites were chosen for high functional connectivity to the amygdala and minimal distance to the vlPFC.

For all participants, TMS was applied to the left PFC at 120% of the individual's pre-scan resting motor threshold. However, the distance between the scalp and the cortex, which influences the strength of the generated electric field at the cortex, typically differs between an individual's primary motor cortex and prefrontal stimulation site. Consequently, the strength of neurostimulation ultimately delivered to the PFC may be less than 120% of motor threshold, if scalp-to-cortex distance is greater at the PFC, or greater than 120%, if scalp-to-cortex distance is greater at M1. We therefore corrected TMS stimulation intensity for within-individual differences in scalp-to-cortex distance at the stimulation site relative to M1 (*39*). We observed that the effective strength of neurostimulation delivered to the left PFC varied across participants (average distance-corrected stimulation intensity = 110% of motor threshold ± 15%). Notably, the effective strength of neurostimulation was significantly positively correlated with the magnitude of the left amygdala TMS evoked response (r_s = 0.35, 95% CI = [0.06 to 0.59], P = 0.0173), providing evidence that relative stimulation level affected the amplitude of the evoked amygdala fMRI response. Absolute stimulator output (% of max) was not correlated with the left amygdala evoked response (r_s = −0.09, 95% CI = [−0.38 to 0.22], P = 0.5764), demonstrating that individually determined motor thresholds corrected for distance may provide more insight into the strength of the electrical field induced at the cortex than raw stimulator output.

Following our a priori analysis of event-related activity in the amygdala ipsilateral to the spTMS application, we additionally explored whether there were TMS effects in the contralateral (right) amygdala. TMS evoked functional responses in the right amygdala were coupled to left amygdala stimulation responses in both direction and amplitude, as revealed by robust correlations between right and left amygdala signed evoked responses (Pearson's r = 0.71, 95% CI = [0.52 to 0.83], P < 0.0001) and absolute valued evoked response magnitudes (Pearson's r = 0.41, 95% CI = [0.14 to 0.63], P = 0.0048). Correspondingly, as in the left amygdala, the TMS evoked response in the right amygdala was significantly negative at the group level (average signed evoked response = −0.08% ± 0.25, t_{44} = −2.04, Cohen's d = 0.30, 95% CI = [−0.15 to −0.001], P = 0.0473), with stimulation pulses resulting in a decrease in right amygdala BOLD signal in 28 participants. Together, these results suggest that lateralized cortical brain stimulation can modulate bilateral amygdala fMRI BOLD activity.

The effects of vlPFC TMS are differentiable across the subcortex

We next sought to assess the specificity of downstream TMS effects within the subcortex. We expected TMS to elicit larger functional responses in the left amygdala than in nontargeted left hemisphere subcortical structures. We thus compared the magnitude of the TMS evoked response in the left amygdala to the magnitude of response in the left caudate, hippocampus, nucleus accumbens, pallidum, putamen, and thalamus. Analyses were conducted on absolute valued TMS evoked responses using a within-subjects design and focused on subcortical regions ipsilateral to the TMS stimulation. We analyzed absolute valued evoked responses here as we were interested in whether the overall size of the TMS effect differed between the amygdala and other subcortical structures irrespective of differences in regional evoked response direction (positive versus negative). spTMS delivered to amygdala functional connectivity peaks located near the left vlPFC induced larger magnitude changes in BOLD signal in the left amygdala than in the left caudate (t_{44} = 4.86, Cohen's d = 0.72, 95% CI = [0.06 to 0.15], P_{FDR} < 0.0001), the left hippocampus (t_{44} = 2.49, Cohen's d = 0.37, 95% CI = [0.01 to 0.07], P_{FDR} = 0.0201), the left pallidum (t_{44} = 4.30, Cohen's d = 0.64, 95% CI = [0.05 to 0.14], P_{FDR} = 0.0003), the left putamen (t_{44} = 4.06, Cohen's d = 0.61, 95% CI = [0.04 to 0.13], P_{FDR} = 0.0004), and the left thalamus (t_{44} = 2.14, Cohen's d = 0.32, 95% CI = [0.003 to 0.10], P_{FDR} = 0.0381). In contrast, evoked responses were smaller in magnitude in the left amygdala than in the left nucleus accumbens, suggesting that the amygdala and accumbens may share TMS-targetable cortical representations (t_{44} = −3.46, Cohen's d = 0.52, 95% CI = [−0.26 to −0.07], P_{FDR} = 0.0018; negative accumbens evoked response in 28 of 45 individuals). Differences in the magnitude of the TMS evoked brain response between the left amygdala and the other six subcortical regions are displayed for each participant in Fig. 2C; most data points fall above the y = 0 line, denoting that evoked responses were consistently larger in amplitude in the amygdala.

To additionally explore whether other subcortical responses to TMS were functionally linked to the amygdala evoked response, we correlated the magnitude of BOLD signal change in the left amygdala with the magnitude of signal change in the aforementioned subcortical structures. Evoked response magnitude in the left amygdala strongly correlated with evoked response magnitude in the left hippocampus (r_s = 0.59, 95% CI = [0.36 to 0.75], P_{FDR} = 0.0001), potentially a result of well-known interregional connections or spatially proximal cortical inputs. Left amygdala evoked responses did not, however, correlate with evoked responses in the left caudate, nucleus accumbens, pallidum, putamen, or thalamus (all P_{FDR} > 0.15), indicating that individual subcortical regions largely display unique functional responses to vlPFC TMS. These findings reveal that the effects of spTMS on the fMRI signal were not only differentiable across subcortical regions but also were almost universally larger in magnitude in the amygdala—the subcortical structure we aimed to target through cortical functional connectivity.

A white matter connection provides a pathway for amygdala modulation

We hypothesized that TMS-induced activation of cortical neurons could exert a downstream influence on the amygdala as a result of action potential propagation along a left prefrontal-amygdala white matter pathway. To retrospectively explore this hypothesis, we first created a group TMS stimulation sites mask that combined the 45

individualized amygdala-targeting sites from all participants. We then generated a whole-brain tractogram from a study-specific FOD template and extracted streamlines with end points in the group stimulation mask and the left amygdala. The use of a study-specific FOD template for white matter delineation and feature analysis offers numerous advantages within the context of this study. Briefly, compared to individual FOD images, the FOD template has increased signal-to-noise and reduced reconstruction uncertainty, and thereby enables superior tractography algorithm performance and more accurate pathway identification. The template furthermore optimizes anatomical correspondence of the studied pathway across participants, eliminating variability in pathway definitions that can be aliased as between-individual differences in microstructural measures. Last, the template approach allows for identification of a population representative pathway that can be compared across species.

Our diffusion MRI analysis identified a white matter pathway connecting anterior portions of the left vlPFC to the left amygdala (Fig. 3A). This structural connection begins in the vlPFC and travels posteriorly before curving downward around medial subcortical structures and projecting through the temporal lobe to the amygdala. Its prefrontal fiber terminations overlap with fibers of the inferior fronto-occipital fasciculus and the uncincate fasciculus, and the pathway stem travels with the anterior thalamic radiation (Fig. 3B). This human vlPFC–amygdala pathway exhibits close correspondence to the main lateral prefrontal-amygdala pathway identified with invasive tract tracing in rhesus macaques (*7*). Specifically, nonhuman primate tract-tracing work has shown that the strongest direct (monosynaptic) projection from the lateral PFC to the amygdala originates within area L12 of the vlPFC in macaques, largely corresponding to Brodmann area 47 (BA47) and anterior BA45 in humans (*10*). Using a Brodmann atlas reconstructed in MRI space (*40*), we determined that 60% of the PFC area occupied by pathway streamline end points localized to BA47 and BA45 (27% to BA10, 13% to anterior/ventral BA46), confirming that our in vivo work recapitulated the spatial pattern of connectivity observed with tract tracing in nonhuman primates. Critically, this left vlPFC–amygdala pathway could function as a causal pathway through which TMS-induced modulation of vlPFC activity produced downstream changes in the ipsilateral amygdala.

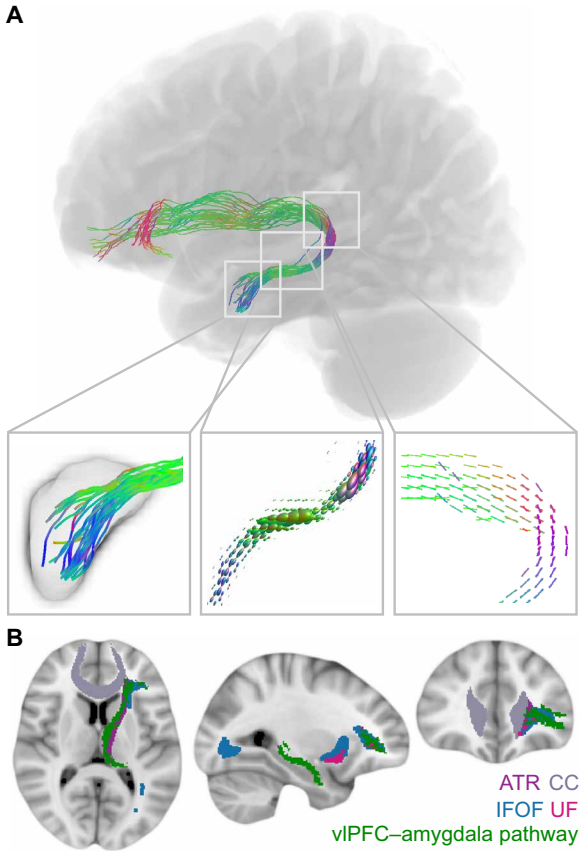

Fig. 3. vlPFC–amygdala white matter pathway anatomy. (**A**) A white matter pathway connecting the left vlPFC stimulation area to the left amygdala could provide a structural scaffold for downstream modulation of the amygdala. This pathway was identified from FOD tractography, and pathway streamlines were mapped to individual fiber bundle elements (fixels) for the calculation of fiber density. The left box displays pathway streamlines terminating in the amygdala. The center box displays pathway FODs scaled by fiber density. The right box displays pathway fixels. Colors represent the fiber direction. (**B**) vlPFC–amygdala white matter pathway trajectory. The identified vlPFC–amygdala pathway is depicted in green overlaid on four major white matter tracts from the JHU ICBM tract atlas including the anterior thalamic radiation (ATR), the corpus callosum (CC), the inferior fronto-occipital fasciculus (IFOF), and the uncinate fasciculus (UF).

Pathway fiber density is associated with the magnitude of the TMS evoked amygdala response

If neurostimulation at the cortex leads to downstream changes in the ipsilateral amygdala fMRI signal by engaging this vlPFC–amygdala white matter pathway, then pathway-derived measures should be associated with the amplitude of the amygdala evoked response. In particular, higher pathway fiber density should enable a larger amygdala evoked response by allowing for more effective signal propagation and enhanced cortical input to the amygdala. To quantify fiber density in the vlPFC–amygdala pathway for each study participant, pathway streamlines were mapped to individual fiber bundle elements (also known as "fixels") in each voxel the pathway traversed, and mean fiber density was estimated across pathway fixels. In support of a circuit-based model of cortical-subcortical TMS signal propagation, individuals with higher fiber density in the left vlPFC–left amygdala white matter pathway exhibited left amygdala TMS evoked responses of significantly greater magnitude ($r_{s.partial}$ = 0.36, 95% CI = [0.07 to 0.60], P = 0.0164) (Fig. 4A). Fiber cross section, a macroscopic, morphological measure of pathway cross-sectional diameter, was not associated with the magnitude of the amygdala evoked response ($r_{s.partial}$ = −0.12, 95% CI = [−0.40 to 0.19], P = 0.4610).

Following this primary analysis, we endeavored to understand whether the vlPFC–amygdala pathway could have been differentially engaged by individuals who responded to TMS with a decrease versus an increase in fMRI activity in the left amygdala. We therefore studied whether the association between pathway microstructure and amygdala evoked response amplitude depended on evoked response direction (positive versus negative). We tested dependence in a linear model with an interaction term between fiber density and response direction for predicting absolute valued response magnitude. The interaction term was not significant ($t_{4,40}$ = 0.47, estimate = 0.79, P = 0.6392), indicating that the relationship between evoked response magnitude and pathway conductivity did not differ between participants exhibiting negative and positive stimulation-induced functional responses in the amygdala. To further confirm the importance of the identified vlPFC–amygdala pathway regardless of amygdala

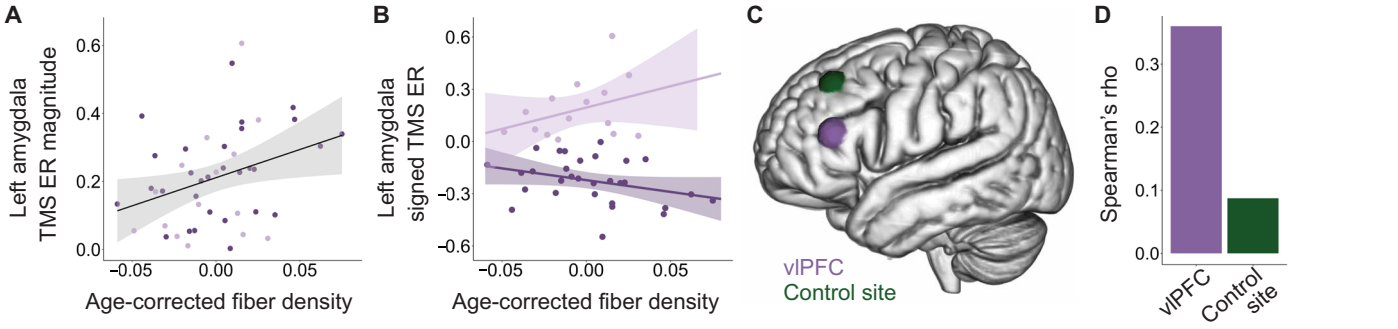

Fig. 4. White matter pathway fiber density affects amygdala TMS evoked responses. (**A**) Across all participants, higher vlPFC–amygdala white matter pathway fiber density was associated with greater absolute valued TMS evoked response (TMS ER) magnitude in the left amygdala. Dark purple circles represent participants that exhibited a negative TMS ER; lighter purple circles represent those that exhibited a positive TMS ER. (**B**) Higher vlPFC–amygdala pathway fiber density was associated with a greater decrease in BOLD signal in individuals that exhibited a negative TMS ER (dark purple) and a greater increase in BOLD signal in individuals that exhibited a positive TMS ER (light purple). (**C**) In addition to the primary spTMS/fMRI scan during which TMS was applied to amygdala-targeting sites near the vlPFC, each participant received an additional spTMS/fMRI scan during which TMS pulses were applied to a secondary active site used in a pathway control analysis. The intensity-weighted center of gravity of all personalized stimulation sites is shown for vlPFC sites (purple) and active control sites (green). (**D**) The strength of the association (rho) between vlPFC–amygdala pathway fiber density and left amygdala TMS ER magnitude was substantially smaller when TMS was applied to active control sites located distant from pathway end points.

evoked response direction, we evaluated the association between pathway fiber density and signed evoked responses independently in groups of negative and positive amygdala responders. When considering only individuals who responded to TMS with a negative evoked response in the left amygdala ($N = 30$), higher fiber density was significantly associated with a larger decrease in left amygdala BOLD signal ($r_{s.partial} = -0.38$, 95% CI = [−0.66 to −0.01], $P = 0.0439$) (Fig. 4B, dark purple). Correspondingly, in the group of positive amygdala responders ($N = 15$), higher pathway fiber density was associated with a larger increase in left amygdala BOLD signal ($r_{s.partial} = 0.27$, 95% CI = [−0.29 to 0.70], $P = 0.3422$) (Fig. 4B, light purple), although this association was not significant, possibly because of an underpowered sample. In all, this set of complementary analyses highlights the utility of studying unsigned evoked response magnitudes and demonstrates that vlPFC–amygdala pathway structural properties were related to cortical-amygdala stimulation propagation across all participants.

In a series of sensitivity analyses, we therefore confirmed that the association between larger left amygdala TMS evoked response magnitude and greater left vlPFC–amygdala pathway fiber density was not driven by the strength of neurostimulation, the strength of baseline stimulation site–amygdala functional connectivity, head motion during scanning, head size, or sex. Sensitivity analyses were conducted across the entire sample, with independent Spearman's rank partial correlations controlling for age plus each potential confounder. The association between pathway fiber density and magnitude of the left amygdala TMS evoked response remained significant when controlling for distance-corrected TMS stimulation intensity ($r_{s.partial} = 0.31$, 95% CI = [0.004 to 0.56], $P = 0.0461$) and the TMS site of stimulation in MNI Y and Z coordinates ($r_{s.partial} = 0.39$, 95% CI = [0.10 to 0.62], $P = 0.0108$). These observations support that individual-tailored elements of the TMS administration did not explain this finding. Given that stimulation sites were selected on the basis of their resting-state functional connectivity with the left amygdala, we verified that the fiber density–amygdala evoked response association could not be attributed to interindividual differences in the strength of this functional connection ($r_{s.partial} = 0.31$, 95% CI = [0.01 to 0.56], $P = 0.0398$). In addition, we showed that the fiber density-amygdala evoked response association was not affected by controlling for head motion during the diffusion scan ($r_{s.partial} = 0.36$, 95% CI = [0.06 to 0.60], $P = 0.0179$), head motion during the spTMS/fMRI scan ($r_{s.partial} = 0.37$, 95% CI = [0.08 to 0.61], $P = 0.0139$), total intracranial volume ($r_{s.partial} = 0.37$, 95% CI = [0.08 to 0.61], $P = 0.0142$), or participant sex ($r_{s.partial} = 0.37$, 95% CI = [0.08 to 0.61], $P = 0.0140$). Last, we verified that using an alternate method for amygdala parcellation did not have an effect on our findings. The association between fiber density and evoked response magnitude was significant when the amygdala was identified using participant FreeSurfer segmentations ($r_{s.partial} = 0.36$, 95% CI = [0.06 to 0.60], $P = 0.0171$), with an effect size equal to that obtained with the Harvard Oxford atlas.

The identified pathway is differentially associated with neurostimulation-induced subcortical responses

Having demonstrated that the magnitude of the left amygdala TMS evoked response was related to fiber density in the delineated pathway, we aimed to establish the specificity of this relationship. We thus examined the association between left vlPFC–amygdala pathway fiber density and spTMS/fMRI BOLD responses in other subcortical structures. Higher vlPFC–amygdala pathway fiber density was also significantly associated with a greater magnitude evoked response in the left hippocampus ($r_{s.partial} = 0.54$, 95% CI = [0.28 to 0.72], $P_{FDR} = 0.0010$), in line with the observation that amygdalar and hippocampal TMS evoked responses were correlated. However, vlPFC–amygdala pathway fiber density was not associated with the magnitude of the evoked response in the left caudate, nucleus accumbens, pallidum, putamen, or thalamus (all $P_{FDR} > 0.90$), suggesting substantial specificity for the influence of the pathway on neurostimulation-induced brain responses in the subcortex.

Pathway fiber density is not related to the TMS evoked amygdala response when stimulating a distant control site

In a final analysis, we investigated whether fiber density in the left vlPFC–amygdala pathway was associated with left amygdala TMS evoked response magnitude when TMS was applied to a second

spatially distant active site. Secondary sites of stimulation used for this pathway control analysis were located dorsally and posteriorly to amygdala-targeting stimulation sites and were positioned, on average, 4.4 (± 1.5) cm away (Fig. 4C). Secondary stimulation sites were designed for a parallel, clinically relevant study assessing downstream effects of spTMS on the subgenual anterior cingulate cortex—a brain region associated with TMS efficacy in depression (*32*, *34*, *35*)—and were therefore selected for exhibiting strong functional connectivity to the subgenual (rather than explicitly for minimal amygdala connectivity). Here, we use these secondary sites as active control sites (i.e., stimulated anatomical controls) to establish whether the vlPFC–amygdala pathway had a dissociable effect on amygdala TMS responses when stimulation was applied close to versus distant from the vlPFC.

spTMS applied to secondary active sites elicited an average absolute value left amygdala evoked response of 0.19% ± 0.25 (negative evoked response in 28 of 45 participants), complementing clinical findings that left dorsolateral TMS can treat disorders typified by amygdala dysfunction, though with variable efficacy (*15*, *16*, *19*). The absolute magnitude of the left amygdala evoked response was larger when stimulating the vlPFC than when stimulating these active control sites in 62% of participants (0.15% larger on average), although this did not represent a statistically significant difference in magnitude ($V = 653$, 95% CI = [−0.01 to 0.10], $P = 0.1284$). We did not identify structural connections between the amygdala and these secondary active TMS sites (using a liberal group mask that combined all participants' subgenual-targeting stimulation sites), suggesting that dorsolateral TMS can affect amygdala activity likely through engagement of polysynaptic connections (*10*). Last, we hypothesized that because stimulation of spatially distant active control sites would be unlikely to directly engage the left vlPFC–amygdala pathway, there would not be a relationship between the microstructure of this white matter pathway and the changes in left amygdala activity elicited by control site TMS. When TMS was applied to the active control sites, vlPFC–amygdala pathway fiber density was not significantly associated with the magnitude of the left amygdala TMS evoked response, causally supporting pathway specificity (Spearman's partial correlation, controlling for age: $r_{s.partial} = 0.09$, 95% CI = [−0.22 to 0.38], $P = 0.5729$) (Fig. 4D).

DISCUSSION

A substantial percentage of individuals experiencing mood, anxiety, and stress-related psychiatric symptoms do not experience a satisfactory clinical response to currently available treatments, necessitating modified or new treatment protocols. A promising, experimental therapeutics-based approach for developing translatable protocols is to identify interventions that are capable of engaging brain regions (targets) strongly linked to symptomatology, such as the amygdala. TMS represents both a psychiatric treatment that can be further optimized and—when combined with fMRI—a tool for measuring target engagement. In the present study, we harnessed interleaved spTMS/fMRI in healthy participants to examine the impact of prefrontal TMS on the amygdala. Our results establish that spTMS delivered within or near the vlPFC elicited acute, stimulation level–dependent modulations of amygdala fMRI BOLD signal. We additionally delineated a phylogenetically conserved white matter pathway connecting the vlPFC to the amygdala with the potential to transmit TMS-induced neural activity from the stimulated cortical surface to the medial temporal lobe. Higher fiber density in the identified pathway was associated with larger magnitude TMS evoked fMRI BOLD responses in the amygdala when stimulating the vlPFC, but not when stimulating an active control site, supporting a specific role for this pathway in vlPFC-to-amygdala TMS signal transduction. Broadly, this spTMS/fMRI probe-and-measure study demonstrates proof of amygdala engagement by TMS and furthermore highlights a potential structural mechanism facilitating engagement of this subcortical target.

Studies investigating the neural bases of psychiatric treatment response have repeatedly reported that reductions in depressive, anxiety, obsessive-compulsive, and posttraumatic stress symptoms occur concomitantly with a normalization of amygdala activity (*17*, *37*, *41*–*44*). Associations between clinical improvement and modified amygdala functioning have been observed following treatment with psychotropics, cognitive behavioral therapy, electroconvulsive therapy, and surgical interventions, convergently suggesting that neuromodulation of the amygdala may facilitate efficacious reductions in transdiagnostic psychopathology. Here, we provide neuromodulation-relevant evidence that TMS applied to left prefrontal-amygdala functional connectivity peaks can evoke a downstream change in amygdala fMRI activity, producing larger effects in the amygdala than in most subcortical regions. In particular, our findings demonstrate that noninvasive brain stimulation engages the amygdala when specifically applied to the vlPFC, a cortical region that is recruited for emotion regulation and transdiagnostically hypoactive in patients with emotion-related psychopathology (*11*, *14*). This represents a replication of our pilot study (*22*) and provides further brain-based evidence identifying the vlPFC territory with axonal projections to the amygdala as a candidate TMS treatment target for mood, anxiety, and stress disorders. Behavior-based evidence corroborating the potential utility of brain stimulation through this circuit is offered by two independent investigations into vlPFC stimulation. In the first investigation, vlPFC TMS facilitated the regulation and reduction of negative emotions in healthy individuals (*45*). In the second investigation, direct electrical stimulation of the anterior vlPFC produced acute improvements in mood in individuals with depression (*46*). Complementary evidence thus indicates that vlPFC stimulation can affect both neural and clinical features that are disrupted across diverse psychiatric disorders. Of note, however, the vlPFC is not the only cortical territory of interest for stimulation-based treatments of amygdala dysfunction. Prior work has shown that repetitive TMS applied to the frontopolar (*47*) or dorsolateral (*18*, *19*) PFC is associated with subsequent changes in amygdala function, and here, spTMS applied to dorsal PFC sites was capable of altering amygdala BOLD signal in some individuals. The relative advantages of ventrolateral, frontopolar, and dorsolateral PFC areas for amygdala-targeted brain stimulation for psychiatric disorders should therefore be further explored. Important advantages of the vlPFC include its role in intentional emotion modulation and reappraisal (*5*–*11*), its accessibility to TMS, and its direct structural pathway to the amygdala that enables robust TMS effects and reliable TMS targeting.

In this study, noninvasive brain stimulation applied to amygdala-targeting cortical sites centered on the vlPFC significantly decreased BOLD signal in the amygdala, inducing an average negative evoked response at the population level. The TMS-induced reduction in fMRI signal was most pronounced in the basolateral amygdala, which includes nuclei involved in fear conditioning, arousal, valuation, and social behavior (*1*–*3*). Given that heightened amygdala activity,

as indexed with fMRI, is consistently observed in persons with psychiatric disorders (*11*, *13*, *14*), this may putatively be the clinically preferred direction of TMS response. It is possible, however, that enhancing amygdala activity may prove beneficial in some contexts. Increases in amygdala neuronal activity are required, for example, for the extinction of conditioned fear (*4*, *48*, *49*). Although TMS pulses reduced overall amygdala activity in most participants, about one-quarter of the study sample did experience a sizeable positive amygdala evoked response, providing evidence for variability in neural responses that could potentially extend to variability in TMS treatment responses. Variability in TMS evoked response direction in the amygdala could not be parsimoniously explained by participant-specific stimulation site properties and may therefore be attributable to interindividual differences in the amygdala neuronal populations engaged by TMS. The amygdala contains populations of excitatory and inhibitory neurons, and its nuclei can furthermore excite and inhibit one another. Consequently, the direction of the signed TMS response likely depends on the precise amygdalar microcircuits that TMS-induced action potentials propagate to, and potentially on the extent to which basolateral versus centromedial and superficial subdivisions are engaged. TMS can also elicit opposing effects on the same brain region depending on the region's current activity state (*26*, *50*–*53*), indicating that contrasting endogenous brain states between participants could also underlie nonuniformity in amgydala evoked response direction.

Irrespective of the direction of the functional response, our data suggest that across all participants, the vlPFC–amygdala white matter pathway contributed to neuromodulation of the amygdala by vlPFC TMS. The vlPFC's structural pathway to the amygdala thus likely allowed TMS to synchronously affect neural activity in both of these regions due to direct depolarization of their axonal connections. The putative importance of directly modulating this vlPFC–amygdala pathway is informed by reports from deep brain stimulation (DBS) in psychiatry: subcortical DBS is significantly more effective at reducing psychiatric symptoms when the electrodes contact cortical-subcortical white matter connections (*54*–*58*). The relevance of this pathway is further underscored by the finding that higher pathway fiber density was associated with larger TMS-induced fMRI activity modulations—yet only within medial temporal lobe subcortical structures and only when stimulating the vlPFC. Our diffusion MRI findings thus provide in vivo evidence that greater white matter conductance enhances the ability of TMS-elicited neural signals to travel to distant brain regions, with white matter connectivity profiles determining the pathway of signal travel. A central role for white matter in shaping downstream responses to TMS highlights the potential for structural connectivity to be harnessed to engage psychopathology-relevant subcortical structures effectively and focally, providing empirical support for the value of diffusion-based TMS targeting.

To date, cortical-subcortical resting-state functional connectivity has been the primary measure considered for targeting subcortical structures with TMS and shows promise for improving clinical outcomes within the context of major depression (*32*, *34*, *35*, *59*). Functional connectivity measured during a clinically relevant task has additionally been proposed as an approach for identifying connectivity-guided TMS sites; this approach was used with an affective pictures task to localize prefrontal-amygdala functional connections to stimulate with repetitive TMS (*47*). Nevertheless, cortical functional connectivity weights for a given subcortical target can vary over time in the same individual, affecting the reproducibility of TMS stimulation site selection (*60*). Structural connectivity is both temporally stable—with white matter pathways forming by early childhood and remaining over the life span—and the underlying physical substrate that allows for signal propagation from cortex to subcortex. Diffusion MRI may thus complement or enhance fMRI for guiding TMS coil positioning. A multimodal approach could be used, for example, to converge on an area of the vlPFC that is both robustly structurally connected to the amygdala and functionally connected to it during an emotion regulation task. Hence, integrative strategies harnessing both structural and functional connectivity are particularly worthy of future study. These personalizable, precision connectomics strategies could eventually be applied not only to enhance the ability of TMS to modulate the amygdala, but also to reach additional subcortical targets that contribute to diverse forms of psychopathology.

The present work must be considered within the context of conventional limitations associated with the acquisition and analysis of spTMS/fMRI and diffusion MRI data. As there are currently no commercially available sham TMS/fMRI coils that mimic the auditory and somatosensory effects associated with in-scanner TMS, this study could not implement a sham control (*26*). We therefore cannot rule out the possibility that TMS-linked increases in perception or arousal contributed to the observed fMRI BOLD effects in the amygdala. We would expect, however, for heightened salience and arousal to both increase activity in the amygdala—yet most participants exhibited a TMS-induced reduction in amygdala fMRI BOLD signal. Future work will benefit from the development of MR-compatible sham coils or stimulation of active controls that exhibit minimal functional connectivity to the amygdala. With respect to the fMRI signal itself, TMS evoked BOLD responses only indirectly index changes in neuronal activity and can additionally be influenced by changes in metabolism, cerebrovascular reactivity, and neurovascular coupling. For our diffusion MRI analysis, the white matter fiber density measure used is not an explicit measure of the number of axons present. However, increases in axon count or packing density (or, potentially, decreases in extracellular space) within a fixel will be reflected as an increase in fiber density. Furthermore, as with all tractography methods, we cannot unequivocally determine whether the structural pathway identified between the left vlPFC and the left amygdala represents a monosynaptic or a polysynaptic connection. Two additional limitations represent key avenues for future investigations. First, this study was not designed to parse whether positive versus negative amygdala TMS evoked responses are predictive of differential behavioral or clinical outcomes to repetitive TMS. Future work should explore relationships between spTMS response directionality and repetitive TMS-induced changes in fear conditioning, negative affect, valence evaluation, or emotion regulation. Second, we used a retrospective study design to examine associations between vlPFC–amygdala white matter pathway features and TMS evoked BOLD responses. Consequently, the TMS coil was not always precisely positioned over the pathway's cortical fiber terminations (e.g., for more dorsally located amygdala-targeting stimulation sites), which could be rectified in a future, prospective structural connectivity–based targeting study.

This study demonstrates that spTMS/fMRI and diffusion MRI can be jointly harnessed to examine how cortical neurostimulation affects the activity in brain regions associated with the manifestation and treatment of psychopathology. Our findings underscore the

relevance of examining downstream, subcortical effects of TMS and the importance of mapping causal circuits underlying these effects. Circuit mapping approaches have been applied in DBS to increase the clinical efficacy of stimulation protocols (*54*–*58*) and, as shown here, can be translated to TMS with the goal of informing treatment protocols. Ultimately, integrating insights derived from spTMS/fMRI brain-based readouts and diffusion-based connectivity into TMS protocols may help to increase the impact of TMS on both brain activity and behavior—thus enhancing the efficacy of therapeutic TMS for psychiatric conditions.

MATERIALS AND METHODS

Experimental design

Healthy participants ages 18 to 55 years with no present or prior reported neurological or psychiatric conditions and no psychotropic medication use participated in this study. All participants gave informed consent before study participation, and all procedures were approved by the University of Pennsylvania Institutional Review Board. All research procedures were performed in accordance with the Declaration of Helsinki. The 45 individuals included in the final study sample had T1-weighted, diffusion, resting-state fMRI, and interleaved spTMS/fMRI data (both amygdala-targeting site and control site data) that passed stringent visual and quantitative quality control procedures. Nine additional individuals had neuroimaging data acquired at the time of analysis but were excluded from the study because of excessive motion or image artifacts. Exclusion criteria included an average relative motion root mean square of >0.15 during spTMS/fMRI scans (four excluded) or an average frame-wise displacement of >0.20 during the diffusion scan coupled with motion-induced patterned slice dropout in diffusion gradients (two excluded) or reconstructed FOD images (three excluded). All neuroimaging data were acquired on the same 3-T Siemens Prisma MRI scanner over two separate scanning days, including a baseline scan day and a TMS/fMRI scan day. During the baseline scan, data from resting-state fMRI, diffusion MRI, and T1-weighted structural MRI sequences were acquired. The resting-state data were collected to identify participant-specific regions in or near the left vlPFC that exhibited strong functional connectivity to the left amygdala. These personalized PFC-amygdala functional connectivity peaks were used as sites of stimulation on the TMS/fMRI scan day. The diffusion MRI data were used to retrospectively evaluate the hypothesis that TMS-induced changes in cortical activity could have a downstream effect on amygdala activity due to a prefrontal-amygdala white matter pathway. Baseline T1-weighted data were used in both fMRI and diffusion analysis streams. During the TMS/fMRI scan day, TMS was applied in the scanner interleaved with fMRI volume acquisitions to quantify evoked changes in amygdala activity in response to single pulses of cortical neurostimulation.

TMS site of stimulation localization: Resting-state fMRI

Baseline resting-state fMRI data were collected to enable fMRI-guided selection of TMS sites of stimulation. Two baseline eyes-open (fixation cross focus) multiband resting-state fMRI scans were acquired with reverse-phase encoding directions in 72 interleaved axial slices with the following acquisition parameters: repetition time = 800 ms, echo time = 37 ms, flip angle = 52°, field of view = 208 mm, voxel size = 2 mm^3, 420 measurements, and multiband acceleration factor = 8. A multiecho T1-weighted MPRAGE scan was additionally acquired with the following parameters: repetition time = 2400 ms, echo time = 2.24 ms, inversion time = 1060 ms, flip angle = 8°, voxel size = 0.8 mm^3, field of view = 256 mm, slices = 208, and Generalized Autocalibrating Partially Parallel Acquisition (GRAPPA) used as a parallel acquisition technique.

T1-weighted scans were processed with the Advanced Normalization Tools (ANTS) Cortical Thickness Pipeline (*61*). Resting-state fMRI data were preprocessed with the eXtensible Connectivity Pipeline Engine (XCP Engine) (*62*) to implement a well-validated, top-performing pipeline for mitigating motion artifacts and noise in fMRI data. Preprocessing steps for the fMRI data included merging of AP and PA acquisitions, removal of the first two volumes from each run to allow for scanner equilibration, realignment of all volumes to an average reference volume, identification and interpolation of time series intensity outliers with AFNI's 3dDespike, demeaning and both linear and polynomial detrending, and registration of fMRI data to T1-weighted data using boundary-based registration. Artifactual variance was modeled as a linear combination of 36 parameters, including 6 motion-related realignment parameters estimated during preprocessing, the mean signal in deep white matter, the mean signal in the cerebrospinal fluid compartment, the mean signal across the entire brain, the first temporal derivatives of the prior 9 parameters, and quadratic terms of both the prior 9 parameters and their derivatives. These 36 nuisance parameters were regressed from the BOLD signal with a general linear model. Last, simultaneous with confound regression, the BOLD time series and the artifactual model time series were temporally filtered (first-order Butterworth) using high-pass-only and low-pass-only filters of >0.01 and <0.08 Hz, respectively. To transform preprocessed fMRI data to MNI space for functional connectivity analysis, T1-weighted images were nonlinearly registered to the MNI T1 template using ANTS symmetric diffeomorphic image normalization (SyN), and transforms were applied to the functional image.

Following preprocessing, functional connectivity—defined as the Fisher's *z*-transformed Pearson correlation coefficient between two BOLD time series—was computed between left frontal cortex voxels and a left amygdala seed, as in prior work (*22*). The amygdala functional connectivity map was then transformed back to participant T1 space and stereotaxically visualized on each participant's curvilinear reconstructed brain surface with neuronavigation (Brainsight; Rogue Research, Montreal, Quebec, Canada). This process allowed for identification of a cortically accessible stimulation site for the in-scanner spTMS/fMRI session that exhibited high functional connectivity to the left amygdala and that localized to (or nearest to) the vlPFC. On the TMS/fMRI scan day, the Brainsight neuronavigation system was used to pinpoint the location on the scalp (marked on a secured lycra swim cap) perpendicular to the amygdala-targeting cortical stimulation site; the TMS coil was centered on this location. Notably, while areas of high amygdala functional connectivity were present within the vlPFC for most participants, prefrontal-amygdala connectivity peaks alternatively localized to the dorsolateral PFC in select individuals. For these individuals, the prefrontal-amygdala functional connectivity peak located in closest proximity to the vlPFC was chosen as the stimulation site. All amygdala-targeting stimulation site coordinates are provided in table S1.

Processed resting-state fMRI data were additionally used to define secondary active sites of stimulation, located in the left middle or superior frontal gyrus, which served as controls for this study. Secondary stimulation sites were designed for a complementary

spTMS/fMRI study investigating the effects of TMS on the subgenual anterior cingulate cortex and were used for a pathway control analysis in the present work. For this reason, secondary stimulation sites were chosen for high functional connectivity to the left subgenual anterior cingulate cortex, rather than for low functional connectivity to the amygdala per se. These sites were selected in Brainsight using seed-to-voxel functional connectivity maps generated with a subgenual seed, as in prior work (*22*).

TMS evoked response quantification: In-scanner, interleaved spTMS/fMRI

We acquired in-scanner interleaved spTMS/fMRI scans while applying TMS with a biphasic pulse to the scalp location that focused stimulation to PFC-amygdala functional connectivity peaks located in closest proximity to the vlPFC. An MRI-compatible TMS coil (MagVenture MRI-B91 air-cooled coil) was positioned to induce a posterior-to-anterior current (first phase), and stimulation intensity was applied at 120% of an individual's resting motor threshold. Resting motor threshold was determined within the MRI room immediately before scanning and defined as the stimulation intensity required to elicit visually observable motor activity in the right hand (in abductor pollicis brevis or first dorsal interosseous muscles) on 5 of 10 consecutive trials. spTMS/fMRI scans were acquired using a TMS-compatible birdcage head coil (RAPID quad T/R single channel; Rimpar, Germany). During scanning, the MRI-B91 TMS coil was connected to a MagPro X100 stimulator (MagVenture; Farum, Denmark) and held firmly in place by a custom-built TMS coil holder. The spTMS/fMRI acquisition parameters included the following: repetition time = 2000 ms, echo time = 30 ms, flip angle = 75°, field of view = 192 mm, voxels = 3 mm by 3 mm by 4 mm, 32 interleaved axial slices, and 178 measurements. Transistor-transistor logic (TTL) trigger pulses sent through a parallel port with E-prime 2.0 (Psychology Software Tools; Sharpsburg, Pennsylvania, USA) were used to control the timing of fMRI volume acquisitions and single TMS pulses. Individual fMRI volume acquisitions were spaced by a 400-ms window during which a single TMS pulse was delivered (triggered at 200 ms). This temporal spacing allows for administration of TMS pulses in a manner that does not contaminate the magnetic field during the subsequent volume acquisition. The spTMS/fMRI scan was broken into 12 spTMS/fMRI mini-blocks throughout which a total of 71 TMS pulses were administered. Each mini-block consisted of seven 400-ms windows during which TMS could be delivered interleaved with seven fMRI volume acquisitions. TMS was administered during five to seven of the mini-block 400-ms windows to incorporate zero to two catch trials, preventing the prediction of when TMS would be delivered. Mini-blocks were separated by seven fMRI volume acquisitions.

Amygdala-targeting spTMS/fMRI data were preprocessed with XCP Engine's task module, which executes the FMRI Expert Analysis Tool (FEAT; version 6.0.0). The functional data were motion-corrected using six standard motion regressors with FSL MCFLIRT, high-pass temporally filtered (cutoff of 100), spatially smoothed (5-mm full width at half maximum kernel), registered to baseline T1-weighted images using boundary-based registration, and transformed to MNI space using precomputed T1-MNI registration transforms. For event modeling, each TMS pulse was considered an instantaneous event and convolved with a gamma-shaped hemodynamic response function. Following model estimation, parameter estimates and contrast values were used to calculate the percent change in BOLD signal from no stimulation (implicit baseline) to stimulation. The average percent BOLD signal change was then quantified in the left hemisphere subcortical structures using the Harvard Oxford subcortical atlas, yielding region-specific TMS evoked responses. We confirmed that this parcellation choice did not affect the quantification of spTMS/fMRI evoked responses by establishing that response estimates were highly similar when defined with the Harvard Oxford atlas and individual FreeSurfer segmentations (Pearson's $r = 0.96$ for Harvard Oxford and FreeSurfer-derived left amygdala TMS evoked response estimates). spTMS/fMRI evoked responses were furthermore quantified within left basolateral, superficial, and centromedial amygdala subdivisions using a discrete parcellation of the histology-based Juelich atlas.

A positive spTMS/fMRI evoked response indicates a TMS-induced increase in BOLD signal, whereas a negative evoked response indicates a TMS-induced decrease in BOLD signal. The magnitude of the spTMS/fMRI evoked response indexes the overall size of the response regardless of direction (i.e., the absolute value) and provides insight into the strength of the functional response elicited by neurostimulation—thereby capturing a main neurobiological effect of interest in this study. Last, on the same TMS/fMRI scan day, a second spTMS/fMRI scan was acquired in a pseudo-random counterbalanced design with TMS targeted to the subgenual anterior cingulate cortex. The subgenual-targeting spTMS/fMRI scan was acquired and processed exactly as detailed above for the amygdala-targeting scan.

Prefrontal-amygdala white matter pathway delineation: Diffusion MRI

Our diffusion MRI analytic workflow sought to determine whether white matter connections originating in the area of cortical stimulation could serve as pathways for TMS-induced signal travel to the amygdala. Diffusion data were acquired in 64 gradient directions with $b = 1000$ s/mm^2 (and one $b = 0$ volume) with the following parameters: repetition time = 4000 ms, echo time = 72.60 ms, flip angle = 90°, voxel size = 2 mm^3, and slice number = 76. The data were preprocessed with QSIPrep 0.6.3RC3, a containerized pipeline that integrates algorithms from diverse software and implements critical preprocessing steps with the best tools available in the field (*63*). In QSIPrep, the data were denoised with Marchenko-Pastur principal components analysis, head motion and eddy currents were corrected using FSL eddy with outlier replacement (*64*), and susceptibility distortions were corrected with field maps generated from magnitude and phase difference images. A nondiffusion weighted reference image ($b = 0$) from the preprocessed diffusion data was registered to a skull-stripped, anterior commissure-posterior commissure (AC-PC) aligned T1-weighted image. A single BSpline interpolation was then applied to both upsample the diffusion data to a 1.3-mm^3 voxel resolution and align it with the AC-PC–realigned T1-weighted image.

All subsequent diffusion analyses, including signal reconstruction with a higher-order diffusion model, tractography, and fixel metric quantification, were implemented following the recommended pipelines in MRtrix3 (*65*) (https://mrtrix.readthedocs.io/en/3.0.0/fixel_based_analysis/st_fibre_density_cross-section.html) using MRtrix3Tissue version 5.2.8 (https://3Tissue.github.io). With MRtrix3Tissue, diffusion images were reconstructed with single-shell three-tissue constrained spherical deconvolution (*66*) using a set of group-averaged white matter, gray matter, and cerebrospinal fluid response functions estimated with the dhollander algorithm (*67*). Constrained spherical deconvolution was implemented for reconstruction, as it allows for the delineation of multiple anatomically accurate fiber populations

per voxel through estimation of a FOD. Each set of antipodally symmetric FOD lobes represents a distinct fiber population; the shape and amplitude of the lobes provide information about fiber microstructure. Critically, the use of three-tissue response functions during deconvolution removes extra-axonal signal contributions from gray matter and cerebrospinal fluid, increasing the precision of the FOD and the biological specificity of the fiber density metric.

Following construction of participant FOD images, images underwent three-tissue bias field correction and global intensity normalization to ensure that absolute FOD amplitudes were directly comparable across all images. A study-specific FOD template was then created using normalized data from all participants. The template was used to conduct FOD-based tractography (iFOD2 algorithm, MRtrix3 default parameters, 2.5 million streamlines), producing a whole-brain tractogram (*68*). Subsequently, streamlines with end points in a group TMS stimulation site mask and a left amygdala mask were extracted—delineating a vlPFC–amygdala structural pathway that could support TMS-induced actional potential propagation. The TMS stimulation site mask was a study-specific mask composed of 1.2-cm-diameter spheres generated around each participant's amygdala-targeting TMS site. This sphere volume was chosen to encompass tissue around the stimulation site likely to have experienced direct suprathreshold neuronal activation while simultaneously maintaining spatial specificity around personalized stimulation sites. The left amygdala was delineated using the Harvard Oxford subcortical atlas. To quantify participant-specific measures within the fiber populations that constitute the extracted vlPFC–amygdala pathway, a fixel-based analysis pipeline was implemented as previously described in detail (*69*). vlPFC–amygdala pathway streamlines were mapped to individual fixels, and each participant's average fiber density and average fiber cross section were calculated across fixels corresponding to the pathway. A primary streamline-to-fixel mapping threshold of five streamlines was used to ensure the robustness of the pathway, in accordance with a prior publication (*70*). We verified, however, that findings were reproducible at mapping thresholds of 2, 4, 6, 8, and 10 streamlines. Fiber density, quantified by the integral of the FOD lobe, is a microstructural measure of a pathway's intra-axonal volume per unit volume of tissue (accounting for crossing fibers) that is sensitive to axon count and packing density (*71*). Fiber cross section is a morphological measure, computed from the Jacobian determinant of a participant-to-template nonlinear warp, which is affected by pathway diameter. Fiber cross section was log-transformed to ensure normality, as advised in the MRtrix3 documentation.

Conducting tractography on a study-specific FOD template rather than on individual participant FOD images confers numerous advantages within the framework of the present study. As compared to individual FOD images, the study-specific FOD template has greatly enhanced signal-to-noise and reduced uncertainty associated with each FOD (*71*). The superior FOD reconstruction quality supports improved tractography performance and lowers susceptibility to spurious streamlines, thus likely increasing the anatomical validity of identified pathways. Extracting streamlines of interest based on a study-specific tractogram also ensures that only white matter pathways that are well represented across the entire study population are analyzed. The delineation of tracts that are highly representative of the population allows for both more apposite across-species comparisons (i.e., between human tractography and macaque tract tracing) and more appropriate comparisons across individuals. Specifically, by optimizing anatomical correspondence of the vlPFC–amygdala pathway across individuals, the template approach ensures that interindividual differences in pathway fiber density cannot simply be attributed to differences in delineation of the pathway itself. This is critical as past work from our group has shown how variability in the extraction of a white matter pathway's streamlines can produce artifactual differences in microstructural measures of interest (*72*). Last, the template approach additionally enables the examination of macrostructural morphological measures that are based on the participant-to-template FOD warp.

Statistical analysis

Statistics were conducted in R 4.0.2. Two-sided, one-sample *t* tests were conducted to determine if, on average, signed TMS evoked responses in the left amygdala, right amygdala, and left amygdala subdivisions (independent tests) were significantly greater or less than 0 when stimulating near the vlPFC. Two-sided, independent samples *t* tests were then conducted to assess whether participants exhibiting negative versus positive amygdala evoked responses differed with respect to stimulation site functional connectivity or anatomical position (*Y* and *Z* coordinates). For subcortical specificity analyses, differences between amygdala evoked response magnitude and evoked response magnitude in other subcortical structures were evaluated with two-sided, paired-sample *t* tests, after confirming normality of paired differences. All *t* tests were performed with the t.test function (stats package in R); corresponding effect sizes were estimated with the cohensD function (lsr package). To compare left amygdala evoked response magnitudes when targeting vlPFC sites versus active control sites, a two-sided paired Wilcoxon signed-rank test (mu = 0) was used, given that the paired differences were non-normally distributed (wilcox.test function, stats package).

Nonparametric Spearman's rank correlations (denoted by r_s) were carried out to determine how correlated the magnitude of the amygdala TMS evoked response was with distance-corrected stimulation intensity and with response magnitude in other subcortical structures. To relate TMS evoked responses to diffusion-derived measures, Spearman's rank partial correlations (denoted by $r_{s.partial}$) controlling for age were used to quantify associations between TMS evoked responses and white matter fiber density or fiber cross section. The fiber cross section analysis additionally included intracranial volume as a covariate, as this morphological measure is strongly correlated with brain size (*73*). Full and partial Spearman's correlations were implemented with cor.test (stats package) and pcor.test functions (ppcor package), respectively; correlation coefficient confidence intervals were estimated with the cor_to_ci function (correlation package). Last, to resolve whether the association between vlPFC–amygdala pathway fiber density and left amygdala TMS evoked response amplitude differed between participants that exhibited negative versus positive amygdala responses, we fit a linear model with absolute valued evoked response magnitude as the dependent variable and both age and an interaction between fiber density and response direction as independent variables (lm function; stats package). Throughout all analyses, false discovery rate correction was applied to correct for multiple comparisons (denoted by P_{FDR}) when multiple subcortical structures were examined in an analysis.

SUPPLEMENTARY MATERIALS

Supplementary material for this article is available at https://science.org/doi/10.1126/sciadv.abn5803

View/request a protocol for this paper from *Bio-protocol*.

REFERENCES AND NOTES

1. J. Gründemann, Y. Bitterman, T. Lu, S. Krabbe, B. F. Grewe, M. J. Schnitzer, A. Lüthi, Amygdala ensembles encode behavioral states. *Science* **364**, eaav8736 (2019).
2. P. H. Janak, K. M. Tye, From circuits to behaviour in the amygdala. *Nature* **517**, 284–292 (2015).
3. M. Pignatelli, A. Beyeler, Valence coding in amygdala circuits. *Curr. Opin. Behav. Sci.* **26**, 97–106 (2019).
4. A. Adhikari, T. N. Lerner, J. Finkelstein, S. Pak, J. H. Jennings, T. J. Davidson, E. Ferenczi, L. A. Gunaydin, J. J. Mirzabekov, L. Ye, S.-Y. Kim, A. Lei, K. Deisseroth, Basomedial amygdala mediates top–down control of anxiety and fear. *Nature* **527**, 179–185 (2015).
5. C. Agustín-Pavón, K. Braesicke, Y. Shiba, A. M. Santangelo, Y. Mikheenko, G. Cockroft, F. Asma, H. Clarke, M.-S. Man, A. C. Roberts, Lesions of ventrolateral prefrontal or anterior orbitofrontal cortex in primates heighten negative emotion. *Biol. Psychiatry* **72**, 266–272 (2012).
6. J. T. Buhle, J. A. Silvers, T. D. Wager, R. Lopez, C. Onyemekwu, H. Kober, J. Weber, K. N. Ochsner, Cognitive reappraisal of emotion: A meta-analysis of human neuroimaging studies. *Cereb. Cortex* **24**, 2981–2990 (2014).
7. H. T. Ghashghaei, C. C. Hilgetag, H. Barbas, Sequence of information processing for emotions based on the anatomic dialogue between prefrontal cortex and amygdala. *Neuroimage* **34**, 905–923 (2007).
8. R. Langner, S. Leiberg, F. Hoffstaedter, S. B. Eickhoff, Towards a human self-regulation system: Common and distinct neural signatures of emotional and behavioural control. *Neurosci. Biobehav. Rev.* **90**, 400–410 (2018).
9. K. N. Ochsner, J. A. Silvers, J. T. Buhle, Functional imaging studies of emotion regulation: A synthetic review and evolving model of the cognitive control of emotion. *Ann. N. Y. Acad. Sci.* **1251**, E1–E24 (2012).
10. R. Ray, D. H. Zald, Anatomical insights into the interaction of emotion and cognition in the prefrontal cortex. *Neurosci. Biobehav. Rev.* **36**, 479–501 (2012).
11. L. M. McTeague, B. M. Rosenberg, J. W. Lopez, D. M. Carreon, J. Huemer, Y. Jiang, C. F. Chick, S. B. Eickhoff, A. Etkin, Identification of common neural circuit disruptions in emotional processing across psychiatric disorders. *Am. J. Psychiatry* **177**, 411–421 (2020).
12. E. Ashworth, S. J. Brooks, H. B. Schiöth, Neural activation of anxiety and depression in children and young people: A systematic meta-analysis of fMRI studies. *Psychiatry Res. Neuroimaging* **311**, 111272 (2021).
13. A. Etkin, T. D. Wager, Functional neuroimaging of anxiety: A meta-analysis of emotional processing in PTSD, social anxiety disorder, and specific phobia. *Am. J. Psychiatry* **164**, 1476–1488 (2007).
14. D. Janiri, D. A. Moser, G. E. Doucet, M. J. Luber, A. Rasgon, W. H. Lee, J. W. Murrough, G. Sani, S. B. Eickhoff, S. Frangou, Shared neural phenotypes for mood and anxiety disorders: A meta-analysis of 226 task-related functional imaging studies. *JAMA Psychiatry* **77**, 172–179 (2020).
15. Q. Guo, C. Li, J. Wang, Updated review on the clinical use of repetitive transcranial magnetic stimulation in psychiatric disorders. *Neurosci. Bull.* **33**, 747–756 (2017).
16. J.-P. Lefaucheur, A. Aleman, C. Baeken, D. H. Benninger, J. Brunelin, V. Di Lazzaro, S. R. Filipović, C. Grefkes, A. Hasan, F. C. Hummel, S. K. Jääskeläinen, B. Langguth, L. Leocani, A. Londero, R. Nardone, J.-P. Nguyen, T. Nyffeler, A. J. Oliveira-Maia, A. Oliviero, F. Padberg, U. Palm, W. Paulus, E. Poulet, A. Quartarone, F. Rachid, I. Rektorová, S. Rossi, H. Sahlsten, M. Schecklmann, D. Szekely, U. Ziemann, Evidence-based guidelines on the therapeutic use of repetitive transcranial magnetic stimulation (rTMS): An update (2014–2018). *Clin. Neurophysiol.* **131**, 474–528 (2020).
17. Y. I. Sheline, D. M. Barch, J. M. Donnelly, J. M. Ollinger, A. Z. Snyder, M. A. Mintun, Increased amygdala response to masked emotional faces in depressed subjects resolves with antidepressant treatment: An fMRI study. *Biol. Psychiatry* **50**, 651–658 (2001).
18. N. Eshel, C. J. Keller, W. Wu, J. Jiang, C. Mills-Finnerty, J. Huemer, R. Wright, G. A. Fonzo, N. Ichikawa, D. Carreon, M. Wong, A. Yee, E. Shpigel, Y. Guo, L. McTeague, A. Maron-Katz, A. Etkin, Global connectivity and local excitability changes underlie antidepressant effects of repetitive transcranial magnetic stimulation. *Neuropsychopharmacology* **45**, 1018–1025 (2020).
19. N. S. Philip, J. Barredo, M. van 't Wout-Frank, A. R. Tyrka, L. H. Price, L. L. Carpenter, Network mechanisms of clinical response to transcranial magnetic stimulation in posttraumatic stress disorder and major depressive disorder. *Biol. Psychiatry* **83**, 263–272 (2018).
20. S. J. H. van Rooij, L. M. Sippel, W. M. McDonald, P. E. Holtzheimer, Defining focal brain stimulation targets for PTSD using neuroimaging. *Depress. Anxiety* **38**, 768–785 (2021).
21. G. A. Fonzo, M. S. Goodkind, D. J. Oathes, Y. V. Zaiko, M. Harvey, K. K. Peng, M. E. Weiss, A. L. Thompson, S. E. Zack, S. E. Lindley, B. A. Arnow, B. Jo, J. J. Gross, B. O. Rothbaum, A. Etkin, PTSD psychotherapy outcome predicted by brain Activation during emotional reactivity and regulation. *Am. J. Psychiatry* **174**, 1163–1174 (2017).
22. D. J. Oathes, J. P. Zimmerman, R. Duprat, S. S. Japp, M. Scully, B. M. Rosenberg, M. W. Flounders, H. Long, J. A. Deluisi, M. Elliott, G. Shandler, R. T. Shinohara, K. A. Linn, Resting fMRI-guided TMS results in subcortical and brain network modulation indexed by interleaved TMS/fMRI. *Exp. Brain Res.* **239**, 1165–1178 (2021).
23. P. M. Rossini, D. Burke, R. Chen, L. G. Cohen, Z. Daskalakis, R. Di Iorio, V. Di Lazzaro, F. Ferreri, P. B. Fitzgerald, M. S. George, M. Hallett, J. P. Lefaucheur, B. Langguth, H. Matsumoto, C. Miniussi, M. A. Nitsche, A. Pascual-Leone, W. Paulus, S. Rossi, J. C. Rothwell, H. R. Siebner, Y. Ugawa, V. Walsh, U. Ziemann, Non-invasive electrical and magnetic stimulation of the brain, spinal cord, roots and peripheral nerves: Basic principles and procedures for routine clinical and research application. An updated report from an I.F.C.N. Committee. *Clin. Neurophysiol.* **126**, 1071–1107 (2015).
24. E. A. Allen, B. N. Pasley, T. Duong, R. D. Freeman, Transcranial magnetic stimulation elicits coupled neural and hemodynamic consequences. *Science* **317**, 1918–1921 (2007).
25. T. Ortuño, K. L. Grieve, R. Cao, J. Cudeiro, C. Rivadulla, Bursting thalamic responses in awake monkey contribute to visual detection and are modulated by corticofugal feedback. *Front. Behav. Neurosci.* **8**, 198 (2014).
26. T. O. Bergmann, R. Varatheeswaran, C. A. Hanlon, K. H. Madsen, A. Thielscher, H. R. Siebner, Concurrent TMS-fMRI for causal network perturbation and proof of target engagement. *Neuroimage* **237**, 118093 (2021).
27. D. Momi, R. A. Ozdemir, E. Tadayon, P. Boucher, M. M. Shafi, A. Pascual-Leone, E. Santarnecchi, Network-level macroscale structural connectivity predicts propagation of transcranial magnetic stimulation. *Neuroimage* **229**, 117698 (2021).
28. D. J. Oathes, N. L. Balderston, K. P. Kording, J. A. DeLuisi, G. M. Perez, J. D. Medaglia, Y. Fan, R. J. Duprat, T. D. Satterthwaite, Y. I. Sheline, K. A. Linn, Combining transcranial magnetic stimulation with functional magnetic resonance imaging for probing and modulating neural circuits relevant to affective disorders. *Wiley Interdiscip. Rev. Cogn. Sci.* **12**, e1553 (2021).
29. J. L. Price, W. C. Drevets, Neural circuits underlying the pathophysiology of mood disorders. *Trends Cogn. Sci.* **16**, 61–71 (2012).
30. L. G. Goetschius, T. C. Hein, W. I. Mattson, N. Lopez-Duran, H. L. Dotterer, R. C. Welsh, C. Mitchell, L. W. Hyde, C. S. Monk, Amygdala-prefrontal cortex white matter tracts are widespread, variable and implicated in amygdala modulation in adolescents. *Neuroimage* **191**, 278–291 (2019).
31. M. Avissar, F. Powell, I. Ilieva, M. Respino, F. M. Gunning, C. Liston, M. J. Dubin, Functional connectivity of the left DLPFC to striatum predicts treatment response of depression to TMS. *Brain Stimul.* **10**, 919–925 (2017).
32. M. D. Fox, R. L. Buckner, M. P. White, M. D. Greicius, A. Pascual-Leone, Efficacy of transcranial magnetic stimulation targets for depression is related to intrinsic functional connectivity with the subgenual cingulate. *Biol. Psychiatry* **72**, 595–603 (2012).
33. L. J. Volz, M. Hamada, J. C. Rothwell, C. Grefkes, What makes the muscle twitch: Motor system connectivity and tms-induced activity. *Cereb. Cortex* **25**, 2346–2353 (2015).
34. A. Weigand, A. Horn, R. Caballero, D. Cooke, A. P. Stern, S. F. Taylor, D. Press, A. Pascual-Leone, M. D. Fox, Prospective validation that subgenual connectivity predicts antidepressant efficacy of transcranial magnetic stimulation sites. *Biol. Psychiatry* **84**, 28–37 (2018).
35. R. F. H. Cash, A. Zalesky, R. H. Thomson, Y. Tian, L. Cocchi, P. B. Fitzgerald, Subgenual functional connectivity predicts antidepressant treatment response to transcranial magnetic stimulation: Independent validation and evaluation of personalization. *Biol. Psychiatry* **86**, e5–e7 (2019).
36. S. Wang, R. Yu, J. M. Tyszka, S. Zhen, C. Kovach, S. Sun, Y. Huang, R. Hurlemann, I. B. Ross, J. M. Chung, A. N. Mamelak, R. Adolphs, U. Rutishauser, The human amygdala parametrically encodes the intensity of specific facial emotions and their categorical ambiguity. *Nat. Commun.* **8**, 14821 (2017).
37. B. R. Godlewska, R. Norbury, S. Selvaraj, P. J. Cowen, C. J. Harmer, Short-term SSRI treatment normalises amygdala hyperactivity in depressed patients. *Psychol. Med.* **42**, 2609–2617 (2012).
38. T. A. Hare, N. Tottenham, M. C. Davidson, G. H. Glover, B. J. Casey, Contributions of amygdala and striatal activity in emotion regulation. *Biol. Psychiatry* **57**, 624–632 (2005).
39. M. G. Stokes, C. D. Chambers, I. C. Gould, T. English, E. McNaught, O. McDonald, J. B. Mattingley, Distance-adjusted motor threshold for transcranial magnetic stimulation. *Clin. Neurophysiol.* **118**, 1617–1625 (2007).
40. R. Pijnenburg, L. H. Scholtens, D. J. Ardesch, S. C. de Lange, Y. Wei, M. P. van den Heuvel, Myelo- and cytoarchitectonic microstructural and functional human cortical atlases reconstructed in common MRI space. *Neuroimage* **239**, 118274 (2021).
41. K. R. Bijanki, S. J. H. van Rooij, T. D. Ely, J. S. Stevens, C. S. Inman, R. E. Fasano, S. E. Carter, S. J. Winters, J. R. Baman, D. L. Drane, T. Jovanovic, J. T. Willie, Case series: Unilateral amygdala ablation ameliorates post-traumatic stress disorder symptoms and biomarkers. *Neurosurgery* **87**, 796–802 (2020).
42. H. Klumpp, J. M. Fitzgerald, Neuroimaging predictors and mechanisms of treatment response in social anxiety disorder: An overview of the amygdala. *Curr. Psychiatry Rep.* **20**, 89 (2018).
43. R. Redlich, C. Bürger, K. Dohm, D. Grotegerd, N. Opel, D. Zaremba, S. Meinert, K. Förster, J. Repple, R. Schnelle, C. Wagenknecht, M. Zavorotnyy, W. Heindel, H. Kugel, M. Gerbaulet, J. Alferink, V. Arolt, P. Zwanzger, U. Dannlowski, Effects of electroconvulsive

therapy on amygdala function in major depression—A longitudinal functional magnetic resonance imaging study. *Psychol. Med.* **47**, 2166–2176 (2017).
44. P. R. Szeszko, R. Yehuda, Magnetic resonance imaging predictors of psychotherapy treatment response in post-traumatic stress disorder: A role for the salience network. *Psychiatry Res.* **277**, 52–57 (2019).
45. D. Cao, Y. Li, Y. Tang, Functional specificity of the left ventrolateral prefrontal cortex in positive reappraisal: A single-pulse transcranial magnetic stimulation study. *Cogn. Affect. Behav. Neurosci.* **21**, 793–804 (2021).
46. V. R. Rao, K. K. Sellers, D. L. Wallace, M. B. Lee, M. Bijanzadeh, O. G. Sani, Y. Yang, M. M. Shanechi, H. E. Dawes, E. F. Chang, Direct electrical stimulation of lateral orbitofrontal cortex acutely improves mood in individuals with symptoms of depression. *Curr. Biol.* **28**, 3893–3902.e4 (2018).
47. L. Beynel, E. Campbell, M. Naclerio, J. T. Galla, A. Ghosal, A. M. Michael, N. A. Kimbrel, S. W. Davis, L. G. Appelbaum, The effects of functionally guided, connectivity-based rTMS on amygdala activation. *Brain Sci.* **11**, 494 (2021).
48. N. W. Lingawi, V. Laurent, R. F. Westbrook, N. M. Holmes, The role of the basolateral amygdala and infralimbic cortex in (re)learning extinction. *Psychopharmacology* **236**, 303–312 (2019).
49. D. C. Knight, C. N. Smith, D. T. Cheng, E. A. Stein, F. J. Helmstetter, Amygdala and hippocampal activity during acquisition and extinction of human fear conditioning. *Cogn. Affect. Behav. Neurosci.* **4**, 317–325 (2004).
50. F. Blankenburg, C. C. Ruff, S. Bestmann, O. Bjoertomt, N. Eshel, O. Josephs, N. Weiskopf, J. Driver, Interhemispheric effect of parietal TMS on somatosensory response confirmed directly with concurrent TMS–fMRI. *J. Neurosci.* **28**, 13202–13208 (2008).
51. S. Borgomaneri, S. Battaglia, S. Garofalo, F. Tortora, A. Avenanti, G. di Pellegrino, State-dependent TMS over prefrontal cortex disrupts fear-memory reconsolidation and prevents the return of fear. *Curr. Biol.* **30**, 3672–3679.e4 (2020).
52. M. S. Hermiller, Y. F. Chen, T. B. Parrish, J. L. Voss, Evidence for immediate enhancement of hippocampal memory encoding by network-targeted theta-burst stimulation during concurrent fMRI. *J. Neurosci.* **40**, 7155–7168 (2020).
53. J. Silvanto, N. G. Muggleton, Testing the validity of the TMS state-dependency approach: Targeting functionally distinct motion-selective neural populations in visual areas V1/V2 and V5/MT+. *Neuroimage* **40**, 1841–1848 (2008).
54. P. Riva-Posse, K. S. Choi, P. E. Holtzheimer, C. C. McIntyre, R. E. Gross, A. Chaturvedi, A. L. Crowell, S. J. Garlow, J. K. Rajendra, H. S. Mayberg, Defining critical white matter pathways mediating successful subcallosal cingulate deep brain stimulation for treatment-resistant depression. *Biol. Psychiatry* **76**, 963–969 (2014).
55. J. C. Baldermann, C. Melzer, A. Zapf, S. Kohl, L. Timmermann, M. Tittgemeyer, D. Huys, V. Visser-Vandewalle, A. A. Kühn, A. Horn, J. Kuhn, Connectivity profile predictive of effective deep brain stimulation in obsessive-compulsive disorder. *Biol. Psychiatry* **85**, 735–743 (2019).
56. N. Li, J. C. Baldermann, A. Kibleur, S. Treu, H. Akram, G. J. B. Elias, A. Boutet, A. M. Lozano, B. Al-Fatly, B. Strange, J. A. Barcia, L. Zrinzo, E. Joyce, S. Chabardes, V. Visser-Vandewalle, M. Polosan, J. Kuhn, A. A. Kühn, A. Horn, A unified connectomic target for deep brain stimulation in obsessive-compulsive disorder. *Nat. Commun.* **11**, 3364 (2020).
57. P. E. Mosley, F. Windels, J. Morris, T. Coyne, R. Marsh, A. Giorni, A. Mohan, P. Sachdev, E. O'Leary, M. Boschen, P. Sah, P. A. Silburn, A randomised, double-blind, sham-controlled trial of deep brain stimulation of the bed nucleus of the stria terminalis for treatment-resistant obsessive-compulsive disorder. *Transl. Psychiatry* **11**, 190 (2021).
58. P. Riva-Posse, K. S. Choi, P. E. Holtzheimer, A. L. Crowell, S. J. Garlow, J. K. Rajendra, C. C. McIntyre, R. E. Gross, H. S. Mayberg, A connectomic approach for subcallosal cingulate deep brain stimulation surgery: Prospective targeting in treatment-resistant depression. *Mol. Psychiatry* **23**, 843–849 (2018).
59. E. J. Cole, K. H. Stimpson, B. S. Bentzley, M. Gulser, K. Cherian, C. Tischler, R. Nejad, H. Pankow, E. Choi, H. Aaron, F. M. Espil, J. Pannu, X. Xiao, D. Duvio, H. B. Solvason, J. Hawkins, A. Guerra, B. Jo, K. S. Raj, A. L. Phillips, F. Barmak, J. H. Bishop, J. P. Coetzee, C. DeBattista, J. Keller, A. F. Schatzberg, K. D. Sudheimer, N. R. Williams, Stanford accelerated intelligent neuromodulation therapy for treatment-resistant depression. *Am. J. Psychiatry* **177**, 716–726 (2020).
60. L. Ning, N. Makris, J. A. Camprodon, Y. Rathi, Limits and reproducibility of resting-state functional MRI definition of DLPFC targets for neuromodulation. *Brain Stimul.* **12**, 129–138 (2019).
61. N. J. Tustison, P. A. Cook, A. Klein, G. Song, S. R. Das, J. T. Duda, B. M. Kandel, N. van Strien, J. R. Stone, J. C. Gee, B. B. Avants, Large-scale evaluation of ANTs and FreeSurfer cortical thickness measurements. *Neuroimage* **99**, 166–179 (2014).
62. R. Ciric, A. F. G. Rosen, G. Erus, M. Cieslak, A. Adebimpe, P. A. Cook, D. S. Bassett, C. Davatzikos, D. H. Wolf, T. D. Satterthwaite, Mitigating head motion artifact in functional connectivity MRI. *Nat. Protoc.* **13**, 2801–2826 (2018).
63. M. Cieslak, P. A. Cook, X. He, F.-C. Yeh, T. Dhollander, A. Adebimpe, G. K. Aguirre, D. S. Bassett, R. F. Betzel, J. Bourque, L. M. Cabral, C. Davatzikos, J. A. Detre, E. Earl, M. A. Elliott, S. Fadnavis, D. A. Fair, W. Foran, P. Fotiadis, E. Garyfallidis, B. Giesbrecht, R. C. Gur, R. E. Gur, M. B. Kelz, A. Keshavan, B. S. Larsen, B. Luna, A. P. Mackey, M. P. Milham, D. J. Oathes, A. Perrone, A. R. Pines, D. R. Roalf, A. Richie-Halford, A. Rokem, V. J. Sydnor, T. M. Tapera, U. A. Tooley, J. M. Vettel, J. D. Yeatman, S. T. Grafton, T. D. Satterthwaite, QSIPrep: An integrative platform for preprocessing and reconstructing diffusion MRI data. *Nat. Methods* **18**, 775–778 (2021).
64. J. L. R. Andersson, M. S. Graham, E. Zsoldos, S. N. Sotiropoulos, Incorporating outlier detection and replacement into a non-parametric framework for movement and distortion correction of diffusion MR images. *Neuroimage* **141**, 556–572 (2016).
65. J.-D. Tournier, R. Smith, D. Raffelt, R. Tabbara, T. Dhollander, M. Pietsch, D. Christiaens, B. Jeurissen, C.-H. Yeh, A. Connelly, MRtrix3: A fast, flexible and open software framework for medical image processing and visualisation. *Neuroimage* **202**, 116137 (2019).
66. J.-D. Tournier, F. Calamante, A. Connelly, Robust determination of the fibre orientation distribution in diffusion MRI: Non-negativity constrained super-resolved spherical deconvolution. *Neuroimage* **35**, 1459–1472 (2007).
67. T. Dhollander, D. Raffelt, A. Connelly, Unsupervised 3-tissue response function estimation from single-shell or multi-shell diffusion MR data without a co-registered T1 image, in *ISMRM Workshop on Breaking the Barriers of Diffusion MRI* (International Society for Magnetic Resonance in Medicine, 2016).
68. J.-D. Tournier, F. Calamante, A. Connelly, MRtrix: Diffusion tractography in crossing fiber regions. *Int. J. Imaging Syst. Technol.* **22**, 53–66 (2012).
69. D. A. Raffelt, J.-D. Tournier, R. E. Smith, D. N. Vaughan, G. Jackson, G. R. Ridgway, A. Connelly, Investigating white matter fibre density and morphology using fixel-based analysis. *Neuroimage* **144**, 58–73 (2017).
70. D. Dimond, C. S. Rohr, R. E. Smith, T. Dhollander, I. Cho, C. Lebel, D. Dewey, A. Connelly, S. Bray, Early childhood development of white matter fiber density and morphology. *Neuroimage* **210**, 116552 (2020).
71. D. A. Raffelt, R. E. Smith, G. R. Ridgway, J.-D. Tournier, D. N. Vaughan, S. Rose, R. Henderson, A. Connelly, Connectivity-based fixel enhancement: Whole-brain statistical analysis of diffusion MRI measures in the presence of crossing fibres. *Neuroimage* **117**, 40–55 (2015).
72. V. J. Sydnor, A. M. Rivas-Grajales, A. E. Lyall, F. Zhang, S. Bouix, S. Karmacharya, M. E. Shenton, C.-F. Westin, N. Makris, D. Wassermann, L. J. O'Donnell, M. Kubicki, A comparison of three fiber tract delineation methods and their impact on white matter analysis. *Neuroimage* **178**, 318–331 (2018).
73. S. Genc, C. B. Malpas, A. Gulenc, E. Sciberras, D. Efron, T. J. Silk, M. L. Seal, Longitudinal patterns of white matter fibre density and morphology in children are associated with age and pubertal stage. *Dev. Cogn. Neurosci.* **45**, 100853 (2020).

Acknowledgments
Funding: This study was supported by National Science Foundation Graduate Research Fellowship DGE-1845298 (to V.J.S.) and by National Institute of Mental Health grants R01MH111886 (to D.J.O.) and RF1MH116920 (to D.S.B., T.D.S., and D.J.O.). **Author contributions:** V.J.S. and D.J.O. designed the study. R.D., J.D., H.L., and M.S. acquired the MRI data. R.D. and M.W.F. processed the structural and resting-state fMRI data and identified TMS stimulation sites, with guidance from D.J.O. V.J.S. processed the diffusion MRI data, with guidance from M.C. V.J.S. implemented all statistical analyses and generated all figures. M.C. conducted an internal code review and technical replication. N.L.B., Y.I.S., D.S.B., T.D.S., and D.J.O. helped with data interpretation and clinical applicability. V.J.S. wrote the manuscript. All authors revised the manuscript. **Competing interests:** The authors declare that they have no competing interests. **Data and materials availability:** All data needed to evaluate the conclusions in the paper are available on dataverse; https://doi.org/10.7910/DVN/TQWRDO. Study analytic code and a guide to code implementation are also available at https://pennlinc.github.io/ZAPR01_dMRI_TMSfMRI/.

Submitted 9 December 2021
Accepted 4 May 2022
Published 22 June 2022
10.1126/sciadv.abn5803